Clim Dyn (2014) 43:1257–1269
DOI 10.1007/s00382-013-1938-y

Impact of Indian summer monsoon on the South Asian High and its influence on summer rainfall over China

Wei Wei · Renhe Zhang · Min Wen · Xinyao Rong · Tim Li

Received: 26 July 2013 / Accepted: 2 September 2013 / Published online: 13 September 2013

Abstract By using the monthly ERA-40 reanalysis data and observed rainfall data, we investigated the effect of the Indian summer monsoon (ISM) on the South Asian High (SAH) at 200 hPa, and the role played by the SAH in summer rainfall variation over China. It is found that in the interannual timescale the east–west shift is a prominent feature of the SAH, with its center either over the Iranian Plateau or over the Tibetan Plateau. When the ISM is stronger (weaker) than normal, the SAH shifts westward (eastward) to the Iranian Plateau (Tibetan Plateau). The east–west position of SAH has close relation to the summer rainfall over China. A westward (eastward) location of SAH corresponds to less (more) rainfall in the Yangtze-Huai River Valley and more (less) rainfall in North China and South China. A possible physical process that the ISM affects the summer rainfall over China via the SAH is proposed. A stronger (weaker) ISM associated with more (less) rainfall over India corresponds to more (less) condensation heat release and anomalous heating (cooling) in the upper troposphere over the northern Indian peninsula. The anomalous heating (cooling) stimulates positive (negative) height anomalies to its northwest and negative (positive) height anomalies to its northeast in the upper troposphere, causing a westward (eastward) shift of the SAH with its center over the Iranian Plateau (Tibetan Plateau). As a result, an anomalous cyclone (anticyclone) is formed over the eastern Tibetan Plateau and eastern China in the upper troposphere. The anomalous vertical motions in association with the circulation anomalies are responsible for the rainfall anomalies over China. Our present study reveals that the SAH may play an important role in the effect of ISM on the East Asian summer monsoon.

Keywords South Asian High · Indian summer monsoon · East Asian summer monsoon · Summer rainfall over China

W. Wei · R. Zhang (✉) · M. Wen · X. Rong
State Key Laboratory of Severe Weather, Chinese Academy of Meteorological Sciences, No. 46 Zhong-Guan-Cun South Ave., Haidian District, Beijing 100081, China
e-mail: renhe@cams.cma.gov.cn

W. Wei
University of Chinese Academy of Sciences, Beijing, China

T. Li
International Pacific Research Center, University of Hawaii at Manoa, Honolulu, HI 96822, USA

1 Introduction

The South Asian High (SAH) is one of the major members of the Asian summer monsoon (ASM) system at upper levels over the South Asian highland (Krishnamurti and Bhalme 1976; Tao and Chen 1987). Affected by the sensible heating from the Tibetan Plateau and the latent heating from the surrounding monsoon regions (Krishnamurti et al. 1973; Huang 1985; Liu et al. 1999, 2001), the SAH is located stably and is the most intense and persistent anticyclone system in the upper troposphere and lower stratosphere in the Northern Hemisphere during boreal summer (Mason and Anderson 1963; Tao and Zhu 1964).

As early as in the 1960s, Mason and Anderson (1963) found the longitudinal shift of SAH when lying over southern Asia in summer. Tao and Zhu (1964) pointed out that the east–west shift of SAH has a quasi-biweekly timescale with the moving direction opposite to that of the Western Pacific Subtropical High (WPSH) at 500 hPa. According to its zonal position, Luo et al. (1982) classified

the SAH into three patterns, named as the east pattern, the west pattern and the zonal (transitional) pattern, which are widely used in the synoptic analysis from then on. They also discussed relationship between the three patterns and the rainfall in eastern China. Based on the climatological pentad mean data, Zhang et al. (2002) revealed the bimodality of the SAH (the Tibetan mode and the Iranian mode) and its difference from the east–west shift in synoptic scale. The rainfall patterns over China associated with these two modes present distinct characteristics.

Some researchers have investigated the impact of the Indian summer monsoon (ISM) on the East Asian summer monsoon (EASM). Guo (1992) found that there is a positive correlation between the summer rainfall in India and in North China. This correlation was reconfirmed by Kripalani and Kulkarni (2001) based on longer time series of rainfall. Zhang (1999) claimed that the impact of ISM on the rainfall in North China is through the transportation of water vapor. Subsequently, Zhang (2001) further pointed out that the water vapor from the ISM exhibits a negative correlation with that from tropical western Pacific associated with the WPSH. When the water vapor from the ISM is less (more) than normal, the rainfall in the Yangtze River Valley is more (less) than normal. Dai et al. (2002) found that the Indian-East Asian pattern teleconnection triggered by huge condensation latent heating from the ISM could influence the rainfall in central and eastern China through affecting the position of WPSH. Wu (2002) and Wu et al. (2003) proposed the role of a mid-latitude wave pattern over Asia in connecting the Indian and North China summer rainfall variations, and the change of the mid-latitude Asian circulation anomaly pattern after the late 1970s may result in a weak relationship between the Indian and the North China summer rainfall (Wu 2002). Ding and Wang (2005) deemed that the ISM may also influence the rainfall in China through ENSO and a global teleconnection at 200 hPa in the middle latitude of the Northern Hemisphere in summer. Moreover, Liu and Ding (2008) put forward a local teleconnection from northwestern India to North China to explain the positive correlation between the ISM and the rainfall in North China.

Many researchers have found that the summer rainfall anomalies in China are related to the location of the SAH (Chen and Liao 1990; Zhang and Wu 2001; Huang and Qian 2003; Wei et al. 2012). As stated above, the SAH is characterized with east–west shift in climatology as well as in the synoptic timescale. However, it is still not clear whether the SAH has the feature of zonal shift in the interannual timescale and what its influence is on the summer rainfall over China. Previous studies have shown that the ISM can affect the EASM. But the role played by the SAH in the effect of ISM on EASM has not been studied yet. Therefore, the present study will explore the characteristics of the interannual east–west shift of the SAH and the impact of ISM on the EASM as well as summer rainfall in China through the SAH. The rest of the paper is organized as follows. Data, method and model used in this study are introduced in Sect. 2. In Sect. 3 the feature of the zonal variation of SAH in the interannual timescale is investigated. The relations of the SAH zonal shift to the EASM and ISM are presented in Sect. 4. In Sect. 5, we discuss the mechanism of the ISM affecting the precipitation in China through the zonal shift of the SAH. Finally, conclusions and discussions are given in Sect. 6.

2 Data, method and model

2.1 Data

The data used in the present study include: monthly mean reanalysis data on a 2.5° × 2.5° horizontal resolution in 1958–2002 derived from the European Centre for Medium-Range Weather Forecasts (ECMWF) (ERA-40) (Uppala et al. 2005); monthly outgoing longwave radiation (OLR) data in the period between 1974 and 2002 on a 2.5° × 2.5° grid from the polar-orbiting series of satellites of the National Oceanic and Atmospheric Administration (Liebmann and Smith 1996); the all-India monthly rainfall data from 1958 to 2002 in the Longest Instrumental Rainfall Series of the Indian Regions from Indian Institute of Tropical Meteorology (Sontakke et al. 1993); observed monthly rainfall data of 160 stations in China from 1958 to 2002 compiled by China Meteorological Administration. Summer mean values are calculated from June to August (JJA) based on the monthly data.

2.2 Method

The apparent heat source Q_1 and the apparent moisture sink Q_2 and their vertically integrated values $\langle Q_1 \rangle$ and $\langle Q_2 \rangle$ are calculated based on the following equations (Yanai et al. 1973; Luo and Yanai 1984):

$$Q_1 = c_p \left[\frac{\partial T}{\partial t} + \vec{V} \cdot \nabla T + \left(\frac{p}{p_0} \right)^{\kappa} \omega \frac{\partial \theta}{\partial p} \right], \quad \langle Q_1 \rangle = \frac{1}{g} \int_{p_t}^{p_s} Q_1 dp \tag{1}$$

$$Q_2 = -L \left[\frac{\partial q}{\partial t} + \vec{V} \cdot \nabla q + \left(\frac{p}{p_0} \right)^{\kappa} \omega \frac{\partial q}{\partial p} \right], \quad \langle Q_2 \rangle = \frac{1}{g} \int_{p_t}^{p_s} Q_2 dp \tag{2}$$

where T is the temperature; θ is the potential temperature; q is the mixing ratio of water vapor, $\vec{V}$ is the horizontal

wind vector; ω is the vertical p-velocity; $\kappa = R/c_p$; R and c_p are the gas constant and the specific heat at constant pressures of dry air, respectively; L is the latent heat of condensation; $p_0 = 1{,}000$ hPa; p_s and p_t are the pressures at the surface and at 1 hPa, respectively.

2.3 Model

An anomalous atmospheric general circulation model (AGCM) (Jiang and Li 2005; Li 2006) is employed in this study to investigate the upper-level circulation responses to the heat source over the ISM region. The model is linearized by specified 3 dimensional summer mean (JJA) basic state, so that model response to specific anomalous heating under the realistic basic mean state could be examined. This anomalous AGCM is at T42 horizontal resolution, and use a sigma ($\sigma = p/p_s$) vertical coordinate with 5 evenly distributed levels from the top level at $\sigma = 0$ to the bottom level at $\sigma = 1$ with an interval of 0.2. Since the mid-latitude circulation response to the heating will be examined in this study, the Newtonian cooling rate of 1 K day^{-1} is applied for the region beyond 50°N and 50°S.

3 Zonal shift of SAH in the interannual timescale

Zhang et al. (2002) documented the statistics of climatological pentad longitude locations of the SAH in summer and found that the center of SAH has the feature of bimodality with one high frequency region lying over the Tibetan Plateau (42.8 %) and the other over the Iranian Plateau (34.4 %). Based on the seasonal mean data in JJA, we analyzed the longitudinal location of the SAH in the interannual timescale and the results are shown in Fig. 1. It can be seen that almost three quarters of the SAH centers in JJA concentrate over the Tibetan Plateau (the Tibetan mode) and about one quarter over the Iranian Plateau (the Iranian mode). We also note that the centers of SAH are seldom located in between. This frequency distribution is similar to the climatological distribution in Zhang et al. (2002) but with more probability over the Tibetan Plateau. That is, the SAH also exhibits bimodal feature in longitude location in the interannual timescale, but prefers to lie over the Tibetan plateau.

Figure 2a shows the climatological geopotential heights at 200 hPa for the summers (JJA) of 45 years from 1958 to 2002. The oval-shaped SAH as outlined by the 12,500-gpm contour bestrides above southern Asia from east to west with its ridge line at about 27.5°N and its center around 85°E. The climatological center of the SAH is slightly to the east of the geometrical center of oval, coinciding with the more frequency of the Tibetan mode as shown in Fig. 1.

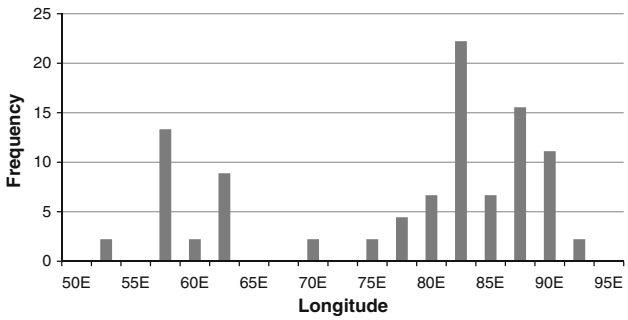

Fig. 1 Longitudinal distribution of the frequency of SAH center locations in JJA from 1958 to 2002 (unit: %)

In order to depict quantitatively the east–west shift of the SAH, two areas, as shown by the dashed boxes in Fig. 2a, Area-A (22.5°–32.5°N, 55°–75°E) and Area-B (22.5°–32.5°N, 85°–105°E) are chosen to calculate the zonal status index. The east–west shift index of SAH (SAHI) is defined as the standardized difference between geopotential heights averaged over Area-B and those averaged over Area-A. The time series of SAHI is shown in Fig. 3. The positive (negative) SAHI indicates that the SAH is located more eastward (westward). The SAHI has a clear feature of interannual variations, indicating the notable east–west shift of the SAH in the interannual timescale.

We choose the SAH with the SAHI higher than 1 as the east mode and lower than -1 as the west mode. As shown in Fig. 3, the east modes of SAH occurred in 1958, 1962, 1965, 1972, 1987 and 1989, while the west modes in 1971, 1973, 1976, 1984, 1994 and 2001. The composites of geopotential heights at 200 hPa for the east and west modes of the SAH are presented in Fig. 2b, c, respectively. For the composite of the east modes with the SAHI higher than 1 (Fig. 2b), the SAH is located eastward with its center over the Tibetan Plateau, and the eastmost point of contour 12,500 gpm extends to 120°E while its westmost point near 37°E. However, for that of the west modes with the SAHI lower than −1 (Fig. 2c), the SAH is located westward with its center over the Iranian Plateau, and the westmost point of contour 12,500 gpm reaches 30°E while its eastmost point at 117°E. It indicates that the SAHI can well depict the zonal displacement of the SAH.

4 Relations of the east–west shift of SAH to rainfall over China and to the ASM

4.1 Rainfall anomalies in China

The composites of summer rainfall in China in the east and west modes of SAH are made respectively and the results

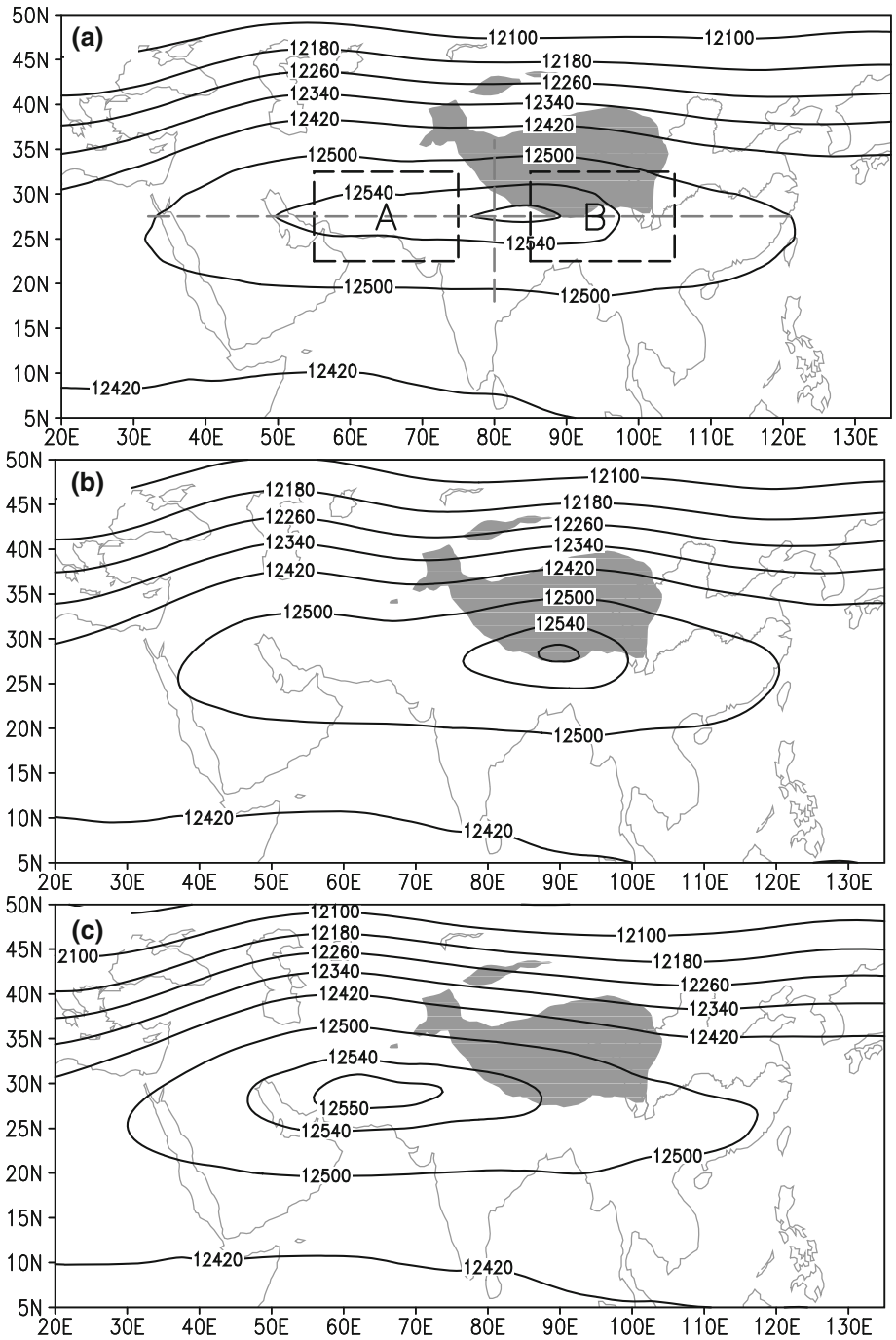

Fig. 2 Geopotential heights at 200 hPa in summer for **a** the climatology as well as the composites for the **b** east and **c** west modes of SAH (unit: gpm). The *dashed box A* (22.5°–32.5°N, 55°–75°E) and *B* (22.5°–32.5°N, 85°–105°E) in **a** illustrate the regions selected to define the east–west shift index of SAH. *Shading* indicates the Tibetan Plateau region with topography exceeding 3,000 m

are shown in Fig. 4. When the SAH is in its east mode (Fig. 4a), the Yangtze-Huai River valley (YHR) is wetter than normal, while North China and the south of the Yangtze River (except the eastern coast) are drier. However, when the SAH is in its west mode (Fig. 4b), there is less rainfall in the middle and lower reaches of the Yangtze River valley, and more rainfall in North China and South China. The difference of composites between the east and west modes of SAH shows that the anomalous rainfall presents a tripole pattern from the north to the south of eastern China (Fig. 4c), which is similar to the first spatial pattern of the EOF analysis (EOF1) on the summer rainfall in China (Zuo et al. 2011). Over many areas the composite differences are statistically significant exceeding the 0.05 significance level according to a Student's *t* test. We also calculate the correlation coefficient between the SAHI and the principal component of EOF1, and it reaches 0.353, exceeding the 0.05 significance level. Obviously, the zonal status of SAH is closely related to the summer rainfall in China, especially the main tripole pattern of rainfall

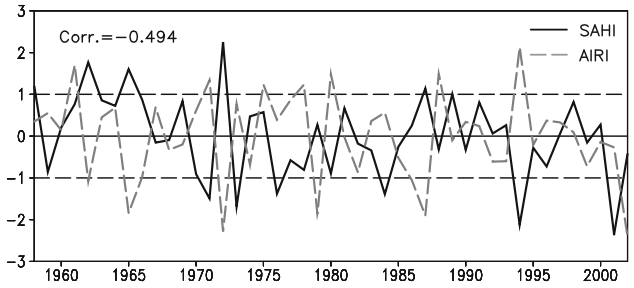

Fig. 3 Standardized time series of SAHI (*solid line*) and AIRI (*dashed line*)

anomalies. The SAHI we defined can well depict the relation of zonal status of SAH to summer rainfall in China.

4.2 Circulation anomalies

The composite differences of the horizontal winds between the east and west modes of SAH at different levels are shown in Fig. 5. At 200 hPa (Fig. 5a), a notable anomalous cyclone is located over the Iranian Plateau and western Tibetan Plateau, while a significant anomalous anticyclone over the eastern Tibetan Plateau and eastern China. The anomalous circulation pattern is similar to that revealed by Wu (2002). The centers of these anomalous circulations are at around 40°N, which are farther north than the SAH ridgeline. As the meridional pressure gradient in middle and high latitudes higher than about 30°N is greater than that in low latitudes lower than about 30°N in the main body of the SAH and to its south, the anomalous signals associated with the SAH zonal displacement are magnified in higher latitudes, inducing more significant circulation anomalies in middle and high latitudes in about 30°–50°N.

The circulation pattern in mid-latitudes at 500 hPa (Fig. 5b) is similar to that at 200 hPa. The anomalous cyclone is still significant over the Iranian Plateau and western Tibetan Plateau but the anomalous anticyclone over the eastern Tibetan Plateau and eastern China becomes weak. Over eastern China, in association with the anomalous anticyclone, anomalous northerly winds prevail, indicating a weaker EASM and a southward shift of the anomalous rainbelt over the YHR in China (Fig. 4c). Additionally, a notable anomalous anticyclone appears over the Indian Peninsula with significant anomalous easterly flow on the southern flank of it, suggesting that the east modes of SAH match with a weak ISM.

At 850 hPa (Fig. 5c), corresponding to a weaker EASM, the WPSH strengthens over southern China and northern South China Sea, leading to less rainfall over southern China. The anomalous southerly winds from the west part of WPSH converge with the anomalous northerly flows

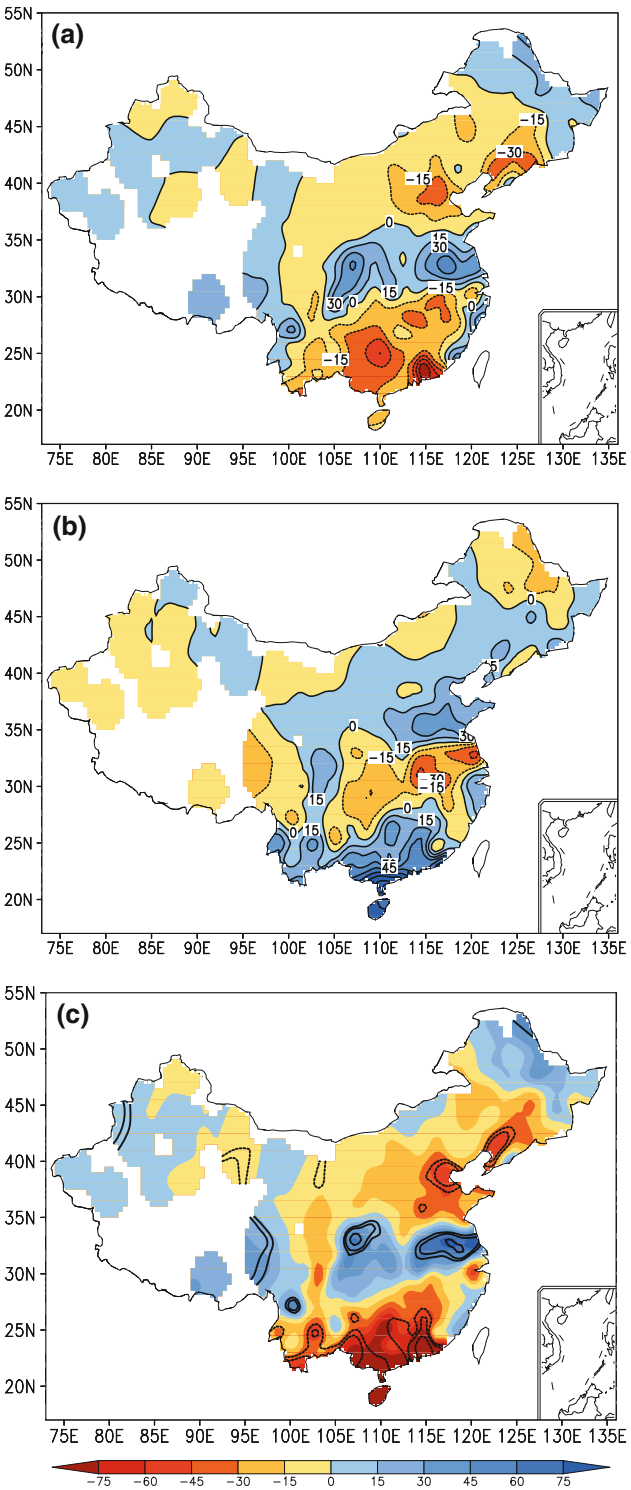

Fig. 4 Composites of rainfall anomalies in China for the **a** east and **b** west modes of SAH, and **c** their difference (unit: mm). *Contours* in **c** indicate significance levels of 0.1, 0.05, and 0.01, respectively

from northern China around the Yangtze River valley and more rainfall appears there. It can be also noticed that there are significant anomalous easterly flows over the Indian Peninsula and Arabian Sea, implying a weaker-than-

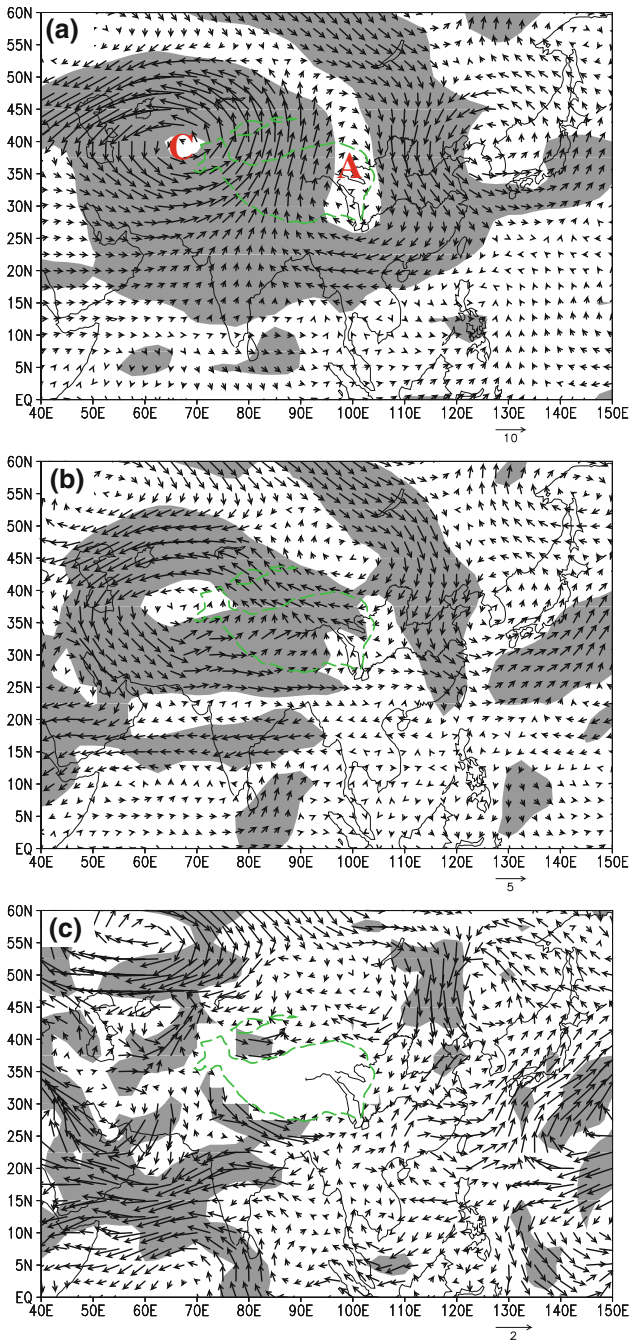

Fig. 5 Composite differences of horizontal winds between the east and west modes of SAH at **a** 200 hPa, **b** 500 hPa and **c** 850 hPa (*vectors*; unit: m s^{-1}). *Shadings* indicate the composite differences exceeding the 0.05 significance level. Contour in *green* indicates the Tibetan Plateau region with topography exceeding 3,000 m

normal ISM. Actually, Zhang (2001) has found a negative correlation of the water vapor transport from the ISM with the rainfall in the middle and lower reaches of the Yangtze River valley, and a positive correlation with the rainfall in North China and South China, which are consistent with what we show in Figs. 4c and 5c.

4.3 Relation of the ISM to the east–west shift of SAH

The composite analyses of circulations in the previous sub-section suggest a close relation of the zonal status of the SAH to the ISM. We will further investigate the influence of the ISM on the SAH in this sub-section. The All Indian Rainfall index (AIRI; Sontakke et al. 1993) is applied to measure the intensity of the ISM. Higher AIRI indicates stronger ISM and more condensation heating over the Indian Peninsula. The interannual variation of the AIRI is shown in Fig. 3. It is shown that there is a significant negative correlation relationship between the SAHI and AIRI. In the extremely anomalous ISM years (e.g. 1965, 1972, 1978, 1987, 1994), the extreme SAHI can also be observed. The correlation coefficient between AIRI and SAHI is −0.494, exceeding the 0.01 significance level. As seen in Fig. 3, there exist weak declined trends in the time series of both SAHI and AIRI. We calculate the correlation coefficient between them after their linear trends are removed. The correlation coefficient becomes larger and reaches −0.567, indicating the negative relationship between the zonal shift of SAH and the ISM is pronounced in the interannual timescale. Here we can see that, when the ISM is stronger than normal with more rainfall in the Indian Peninsula, the SAH moves westward. Contrarily, when the ISM is weaker, the SAH moves eastward.

Due to the direct relationship between the rainfall and convection in lower latitudes, we utilize the OLR to investigate the ISM activities. Figure 6 gives the regressed OLR against the SAHI during the period from 1974 to 2002. Positive OLR anomalies exceeding the 0.05 significance level cover from the south of Iranian Plateau, northern Indian Peninsula, to the northern Bay of Bengal. It indicates that the convective activities in ISM region are closely related to the SAH zonal shift, coinciding with the results revealed by the Indian rainfall. Meanwhile, over eastern China the tripole distribution of OLR anomalies can be clearly seen, which corresponds well to the rainfall anomalies shown in Fig. 4. It indicates that when the rainfall is below (above) normal and the convective activities are weak (strong) over ISM region, the SAH is in its east (west) mode. On the contrary, when the rainfall is more than normal and the convective activities are strong, the SAH is in its west mode.

5 Possible mechanism of the ISM influencing the EASM

The previous section has shown that the zonal displacement of SAH, which is related to the summer rainfall anomalies in China, is significantly influenced by the ISM. In this section, we will explore the physical process by which the ISM affects summer rainfall in China through the zonal displacement of the SAH.

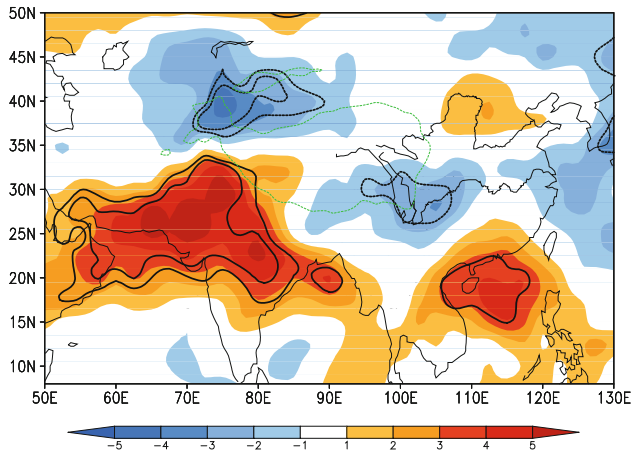

Fig. 6 Regressed OLR against SAHI (*shadings*; unit: w m^{-2}). Areas exceeding the 0.05 and 0.01 significance levels are highlighted by *dark contours*. *Contour* in *green* indicates the Tibetan Plateau region with topography exceeding 3,000 m

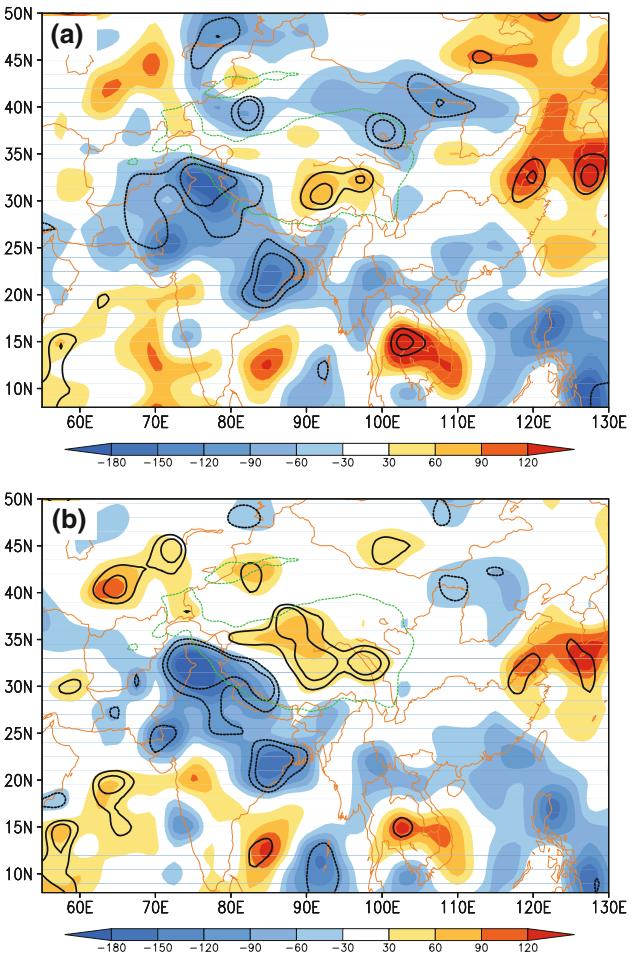

Fig. 7 Composite differences between the east and west modes of SAH for the **a** integrated apparent heat source $\langle Q_1 \rangle$ and **b** apparent moisture sink $\langle Q_2 \rangle$ (unit: w m^{-2}). Areas exceeding the 0.05 and 0.01 significance levels are highlighted by *thick lines*. *Contour* in *green* indicates the Tibetan Plateau region with topography exceeding 3,000 m

5.1 Effect of ISM on the zonal displacement of SAH

5.1.1 Diagnostic analysis

As a thermodynamic high in the upper troposphere, the formation and movement of the SAH is affected by both the surface and atmosphere heating (Krishnamurti et al. 1973; Huang 1985; Liu et al. 1999, 2001; Zuo et al. 2011; Wu et al. 2013). The heating differences between the east and west modes of SAH will be analyzed here to explore the possible cause of the zonal displacement of the SAH.

The integrated apparent heat source $\langle Q_1 \rangle$ represents the total effect of the radiation, sensible heating and latent heating. And the integrated apparent moisture sink $\langle Q_2 \rangle$ is mainly related to the condensation latent heating. Figure 7 gives the composite differences of $\langle Q_1 \rangle$ and $\langle Q_2 \rangle$ between the east and west modes of SAH, respectively. It can be seen that there are pronounced negative anomalies over the northern Indian Peninsula for both $\langle Q_1 \rangle$ and $\langle Q_2 \rangle$. In addition, the values of $\langle Q_1 \rangle$ and $\langle Q_2 \rangle$ are nearly equivalent, implying that the heating anomalies over the northern Indian Peninsula are mainly condensation latent heating induced by convection. When the SAH is in its east mode, the condensation heating is weaker than normal because of the less rainfall over the ISM region, and vice versa. These results are consistent with the anomalous OLR shown in Fig. 6.

Over the Tibetan Plateau, the positive anomalies of $\langle Q_1 \rangle$ and $\langle Q_2 \rangle$ are also significant, but the anomalous $\langle Q_1 \rangle$ extends not as broadly as the $\langle Q_2 \rangle$ does, and their centers are not lying over the same place. These features indicate that the heating over the Tibetan Plateau is not only contributed by the latent heating, but also by the sensible heat or others. Moreover, heat source over the Tibetan Plateau is much weaker and plays an opposite role in affecting the SAH zonal displacement compared to that over the Indian Peninsula. By comparing the deep convection activities over the Tibetan Plateau to those over the ISM regions, Luo et al. (2011) found that the frequency, vertical and horizontal scales of deep convection over the Indian monsoon region are larger than those over the Tibetan Plateau. Therefore, the release of latent heat by condensation of deep convection over the Indian Peninsula plays a dominant role in affecting the zonal displacement of the SAH.

In order to explain the effect of the atmospheric heating on circulations, a simplified vorticity equation is applied and expressed as (Liu et al. 1999, 2001):

$$\beta v \propto \frac{f+\zeta}{\theta_z}\frac{\partial Q}{\partial z}, \quad \theta_z \neq 0 \tag{3}$$

where Q is the diabatic heating, ζ is the vertical vorticity, and θ_z is static stability.

In the upper troposphere over the maximum heating center, $\frac{f+\zeta}{\theta_z}\frac{\partial Q}{\partial z} < 0$, and the northerly winds will appear at high levels according to Eq. 3, inducing an anticyclone to the west and a cyclone to the east (Liu et al. 1999, 2001). Therefore, the strong anomalous southerlies as well as the anomalous cyclone to the west and anomalous anticyclone to the east at 200 hPa (Fig. 5a) can be explained by the negative anomalous heating over the north of the Indian Peninsula (Fig. 7) because $\frac{f+\zeta}{\theta_z}\frac{\partial Q}{\partial z} > 0$ in the upper troposphere. It implies that the anomalous latent heating over the northern Indian Peninsula due to the anomalous ISM is the main contributor of the zonal displacement of the SAH, as well as the anomalous circulations in middle latitudes at 200 hPa.

5.1.2 Numerical experiments

By utilizing the anomalous AGCM (Jiang and Li 2005; Li 2006), we conduct numerical experiments to further confirm the effect of the latent heating from the rainfall condensation over ISM region on the zonal displacement of the SAH.

Two idealized numerical experiments, the positive heating run (PHR) and the negative heating run (NHR) are conducted. According to the observed vertical profile of the Q_1, in the PHR we adopted a vertical profile of the ideal heating anomaly as shown in Fig. 8a. The largest diabatic heating anomaly of 1 K day^{-1} is placed over the northern Indian Peninsula at the level $\sigma = 0.5$, and its horizontal distribution are shown in Fig. 8b. The horizontal heating center is taken to be at 30°N, 78°E. As seen in Fig. 7a, the negative anomalies of Q_1 appear over northern India with three centers located at about (72°E, 26°N), (77°E, 32°N), and (84°E, 22°N), respectively. The latitude of the horizontal heating center in our numerical experiments is a little higher than the averaged latitude of these three centers because the strongest negative center with -180 w m^{-2} is located at 77°E, 32°N (Fig. 7a). The experiments are conducted by running the AGCM for 24 months under fixed summer basic state, and the ensemble mean of the last 20 months is used to analyze the responses of upper-level circulations to the prescribed heating source. The NHR is the same as the PHR, but with a negative heating anomaly over the northern Indian Peninsula by multiplying -1 to the vertical profile of the heating anomaly.

The difference of the horizontal winds at 200 hPa between the ensemble mean of the NHR and that of the PHR is shown in Fig. 8b. The circulation pattern induced by the diabatic heating over the northern Indian Peninsula is quite similar to the observed results shown in Fig. 5a. The heating anomaly above the Indian Peninsula triggers the anomalous cyclone to the northwest of the heat source and the anomalous anticyclone to the northeast, covering the eastern Tibetan Plateau and eastern China. The anomalous southerly winds obviously appear over the heat source, in consistency with the proportional relationship between the meridional wind and the vertical gradient of the diabatic heating discussed in above subsection. It further proves that

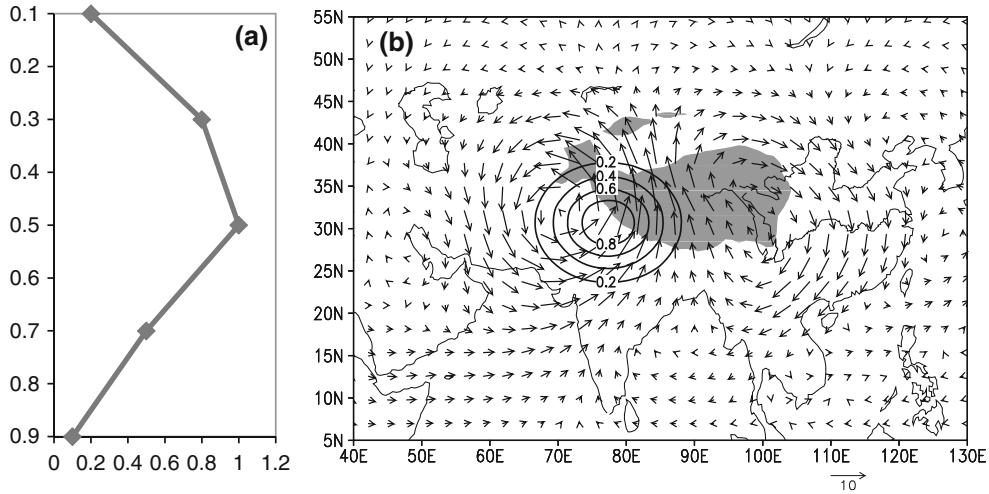

Fig. 8 **a** Vertical profile of the ideal heating anomaly prescribed in the PHR, and in the NHR the heating anomaly is multiplied by -1 (unit: K day^{-1}). **b** Difference of ensemble horizontal winds between the NHR and PHR at 200 hPa (*vectors*; unit: m s^{-1}). *Contours* in **b** indicate the horizontal distribution of the diabatic heating (unit: K day^{-1}). *Shading* indicates the Tibetan Plateau region with topography exceeding 3,000 m

the latent heat anomaly associated with ISM is the main cause of the zonal displacement of the SAH.

5.2 Effect of the zonal variation of SAH on the rainfall in China

Because the vertical motion is closely related with rainfall, in Fig. 9 we show the composite difference between the east and west modes of SAH for the vertical velocity and vertical circulation over eastern China. The ascending motion with negative anomalies of ω appears in 27.5°–35°N over the YHR, while descending motions are found over 37.5°–42.5°N and 20°–27°N, respectively. Compared to the anomalous rainfall pattern shown in Fig. 4c, the ascending and descending motions correspond well to the increased rainfall over the YHR and suppressed rainfall in North China and South China, respectively. Here we can see that the rainfall anomalies are mainly determined by the vertical motions. In the following we will use the quasi-geostrophic omega equation (Eq. 4) to diagnose the formation mechanism of the vertical motions.

The quasi-geostrophic omega equation is taken as

$$\left(\sigma\nabla^2+f_0^2\frac{\partial^2}{\partial p^2}\right)\omega=f_0\frac{\partial}{\partial p}\left[\vec{V}_g\cdot\nabla(\zeta_g+f)\right]+\frac{R}{p}\nabla^2\left[\vec{V}_g\cdot\nabla T\right], \tag{4}$$

Oort 1984). Then Term B and Term C in Eq. 4 can be written as:

$$\begin{aligned} &f_0\frac{\partial}{\partial p}\left[\vec{V}_g\cdot\nabla(\zeta_g+f)\right]\\ &=f_0\frac{\partial}{\partial p}\left[\left(\overline{\vec{V}_g}+\vec{V}_g{}'\right)\cdot\left[\nabla\left(\overline{\zeta_g}+\zeta_g'\right)+\frac{\partial f}{\partial y}\right]\right]\\ &=f_0\frac{\partial}{\partial p}\left[\left(\overline{u_g}\frac{\partial\overline{\zeta_g}}{\partial x}+u_g'\frac{\partial\overline{\zeta_g}}{\partial x}+\overline{u_g}\frac{\partial\zeta_g'}{\partial x}+u_g'\frac{\partial\zeta_g'}{\partial x}\right.\right.\\ &\quad\left.\left.+\overline{v_g}\frac{\partial\overline{\zeta_g}}{\partial y}+v_g'\frac{\partial\overline{\zeta_g}}{\partial y}+\overline{v_g}\frac{\partial\zeta_g'}{\partial y}+v_g'\frac{\partial\zeta_g'}{\partial y}\right)+\left(\overline{v_g}\frac{\partial f}{\partial y}+v_g'\frac{\partial f}{\partial y}\right)\right] \end{aligned} \tag{4a}$$

$$\begin{aligned} \frac{R}{p}\nabla^2\left[\vec{V}_g\cdot\nabla T\right]&=\frac{R}{p}\nabla^2\left[\left(\overline{\vec{V}_g}+\vec{V}_g'\right)\cdot\nabla(\bar{T}+T')\right]\\ &=\frac{R}{p}\nabla^2\left(\overline{u_g}\frac{\partial\bar{T}}{\partial x}+u_g'\frac{\partial\bar{T}}{\partial x}+\overline{u_g}\frac{\partial T'}{\partial x}+u_g'\frac{\partial T'}{\partial x}\right.\\ &\quad\left.+\overline{v_g}\frac{\partial\bar{T}}{\partial y}+v_g'\frac{\partial\bar{T}}{\partial y}+\overline{v_g}\frac{\partial T'}{\partial y}+v_g'\frac{\partial T'}{\partial y}\right) \end{aligned} \tag{4b}$$

where the variables with bar and prime are their basic state and perturbation, respectively. Considering that the basic state variables themselves satisfy the equation, the omega equation of perturbation can be written as:

$$\begin{aligned} \left(\sigma\nabla^2+f_0^2\frac{\partial^2}{\partial p^2}\right)\omega'=&\underbrace{f_0\frac{\partial}{\partial p}\left(u_g'\frac{\partial\overline{\zeta_g}}{\partial x}\right)}_{\mathbf{B1}}+\underbrace{\overline{u_g}\frac{\partial\zeta_g'}{\partial x}}_{\mathbf{B2}}+\underbrace{u_g'\frac{\partial\zeta_g'}{\partial x}}_{\mathbf{B3}}+\underbrace{v_g'\frac{\partial\overline{\zeta_g}}{\partial y}}_{\mathbf{B4}}+\underbrace{\overline{v_g}\frac{\partial\zeta_g'}{\partial y}}_{\mathbf{B5}}+\underbrace{v_g'\frac{\partial\zeta_g'}{\partial y}}_{\mathbf{B6}}+\underbrace{v_g'\frac{\partial f}{\partial y}}_{\mathbf{B7}}\\ &+\underbrace{\frac{R}{p}\nabla^2\left(u_g'\frac{\partial\bar{T}}{\partial x}\right)}_{\mathbf{C1}}+\underbrace{\overline{u_g}\frac{\partial T'}{\partial x}}_{\mathbf{C2}}+\underbrace{u_g'\frac{\partial T'}{\partial x}}_{\mathbf{C3}}+\underbrace{v_g'\frac{\partial\bar{T}}{\partial y}}_{\mathbf{C4}}+\underbrace{\overline{v_g}\frac{\partial T'}{\partial y}}_{\mathbf{C5}}+\underbrace{v_g'\frac{\partial T'}{\partial y}}_{\mathbf{C6}} \end{aligned} \tag{5}$$

where all operators and variables are of conventional usage in meteorology. The term on the left hand side of Eq. 4 is the Laplacian of omega (called as Term A) and approximately equivalent to omega multiplied by a negative coefficient. The terms on the right hand side are the vertical differential of geostrophic absolute vorticity advection (called as Term B) and the Laplacian of geostrophic temperature advection (called as Term C), respectively. Each variable in Eq. 4 can be divided into a time-averaged basic state and its departure (Peixóto and

The level 500 hPa can be regarded as a non-divergence level, which is most suitable to diagnose the vertical motions. Therefore, we choose 500 hPa to diagnose the vertical motions by calculating each term on the right hand side of Eq. 5 as denoted by B1–B7 and C1–C6 in domains 35°–42.5°N, 110°–120°E and 27.5°–35°N, 110°–120°E respectively, to find out the main contributors to the vertical motion anomalies over North China and the YHR.

As shown in Fig. 10, the results reveal that the terms B2 and C4 in Eq. 5 are 2 main contributors to the downdraft

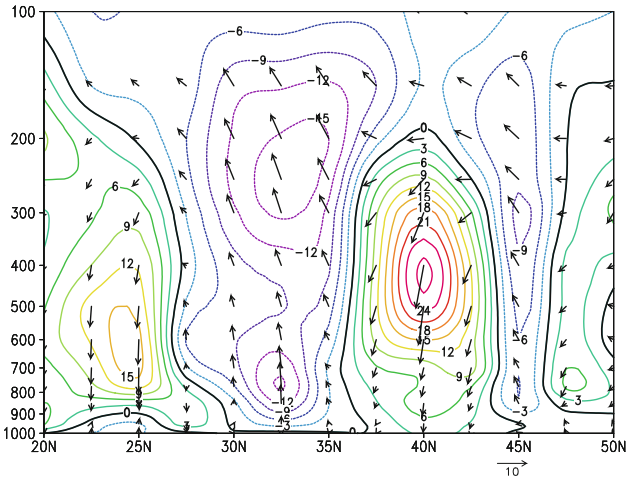

Fig. 9 Latitude-height cross-section of the composite differences between the east and west modes of SAH for vertical velocity (*contours*; unit: 0.001 Pa s^{-1}) and vertical circulation (*vectors*; the unit of the meridional wind is m s^{-1}; the p-velocity has been multiplied by 500) along 110°–120°E

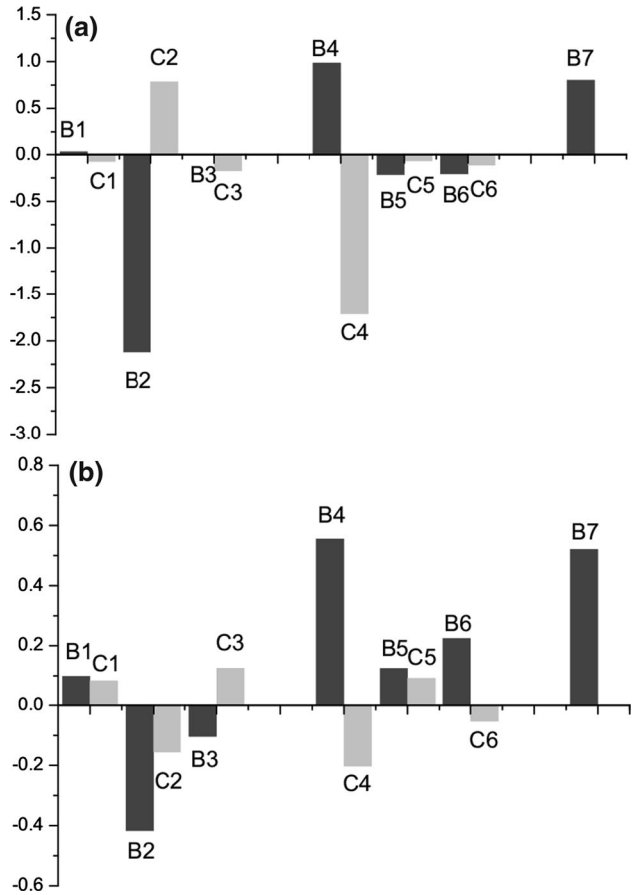

Fig. 10 Composite differences between the east and west modes of SAH at 500 hPa for 7 terms of $f_0 \frac{\partial}{\partial p}\left[\vec{V}_g \cdot \nabla(\zeta_g + f)\right]$ denoted by B1–B7 (*dark grey*) and 6 terms of $\frac{R}{p}\nabla^2\left[\vec{V}_g \cdot \nabla T\right]$ denoted by C1–C6 (*light grey*) averaged over **a** North China (35°–42.5°N, 110°–120°E) and **b** the YHR (27.5°–35°N, 110°–120°E) (unit: 10^{-19} m s^{-1} kg^{-1})

anomalies over North China (Fig. 10a), while the terms B4 and B7 to the updraft anomalies over the YHR (Fig. 10b). In fact, these terms can be well reflected by the pattern of anomalous circulations showing in Fig. 5b. The term B2 is closely related to the advection by the basic zonal flow to the anomalous relative vorticity associated with the anomalous anticyclone over the eastern Tibetan Plateau and eastern China. The terms B4 and C4 as well as B7 are the advections of the basic relative vorticity and temperature as well as the vorticity of the earth, respectively, by the anomalous northerly winds over eastern China on the east flank of the anomalous anticyclone.

Since the four terms of advections are related to the basic states of relative vorticity ($\bar{\zeta}_g$), temperature ($\bar{T}$) and horizontal wind ($\overrightarrow{\bar{V}_g}$), in Fig. 11 we show their basic state fields at 500 hPa averaged in JJA for further illustrating the effect of them on the vertical motions. In the eastern China over the area 27.5–42.5°N, 110–120°E, the westerly basic winds prevail, which make advection of the negative vorticity associated with the anomalous anticyclone and result in descending motion as denoted by the term B2. The meridional gradient of the basic temperature is reversed to that of the basic relative vorticity, so that the roles of their advections by the anomalous northerly winds in vertical motions are of opposite effect, leading to updraft for the term B4 and downdraft for C4. Since the higher the latitude, the larger the Coriolis parameter f, the advection of the vorticity of the earth by the anomalous northerly winds denoted by the term B7 has the same effect on vertical motion as the term B4. The downdraft effects by the terms B2 and C7 are larger than the updraft effects by the terms B4 and B7 in North China (Fig. 10a), but reversed effects on vertical motions can be found in the YHR (Fig. 10b). As a result, in the east mode of SAH, both of the cold advection by the anomalous northerly winds and the advection of anomalous negative relative vorticity by the westerly basic winds cause the anomalous descending motion over North China, while the advections of the positive basic relative vorticity and the positive vorticity of the earth by the anomalous northerly winds lead to the anomalous ascending motion over the YHR.

Being close to the tropic, the quasi-geostrophic omega equation could not be used to diagnose the vertical motion over South China. Figure 9 shows a meridional circulation with the updraft over the YHR and the downdraft over South China. The composites of WPSH at 500 hPa in the east and west modes of SAH is displayed respectively in Fig. 12. In the east mode the WPSH is westward extended and a further southward ridge line lies at about 24°N. The South China is controlled by the WPSH, so that the descending motion appears over there and the rainfall is

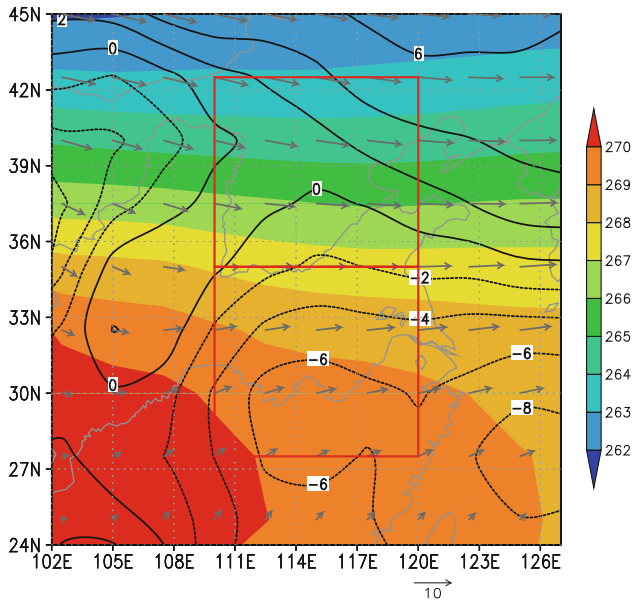

Fig. 11 Basic state fields of relative vorticity (*contours*; unit: 10^{-6} s^{-1}), temperature (*shadings*; unit: K), and horizontal winds (*vectors*; unit: m s^{-1}) at 500 hPa averaged in JJA. The *red boxes* indicate the regions of North China (35°–42.5°N, 110°–120°E) and the YHR (27.5°–35°N, 110°–120°E), respectively

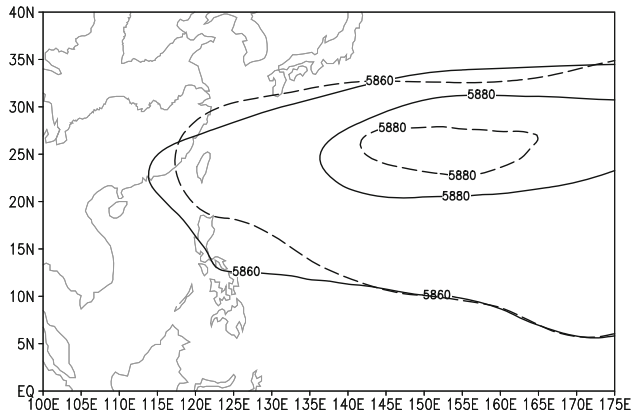

Fig. 12 Composites of the WPSH (denoted by 5,880 gpm) at 500 hPa in the east (*solid*) and west (*dashed*) modes of SAH

suppressed. In the west mode the WPSH is located northward with the ridge line near 27°N. The South China can be affected by the depression systems from tropics, leading to positive rainfall anomalies.

6 Conclusions and discussions

Statistical analyses based on the seasonal mean data of JJA from 1958 to 2002 show that the zonal shift of the SAH is significant in summer in the interannual timescale. The center of SAH at 200 hPa usually appears either above the Iranian Plateau or above the Tibetan Plateau, and is seldom located in between. An index of SAH (SAHI) is defined to measure the zonal displacement of the SAH, and two types of SAH of pronounced eastward shift (east mode) and westward shift (west mode) are classified based on the SAHI.

The zonal status of SAH is closely related to a tripole pattern of the summer rainfall anomalies in eastern China. In the east mode of SAH the YHR is wetter than normal while North China and the southern China are drier, and in the west mode the anomalous rainfall pattern is almost opposite. Besides, by utilizing both the rainfall and convection data over Indian summer monsoon region, we demonstrate a significant negative correlation relationship between the SAH zonal shift and the ISM, suggesting the impact of the ISM on the SAH and thus the EASM.

In the east mode of SAH, it can be observed that at 200 hPa a notable anomalous cyclone is located over the Iranian Plateau and western Tibetan Plateau, while a significant anomalous anticyclone over eastern Tibetan Plateau and eastern China. Diagnostic analysis and numerical experiments are used to investigate the physical process of the influence of the ISM on the zonal status of the SAH. In summer, the east mode of SAH is often found in weak ISM. The inactive convection over the Indian Peninsula leads to anomalous condensation cooling in the upper troposphere. According to a simplified vorticity equation, the increasing heating rate against altitude in the upper troposphere over the anomalous cooling region can induce anomalous southerly winds in the upper troposphere over the area of cooling region, which are favorable for anomalous cyclone and anticyclone appearing in pairs to the northwest and northeast of the heating anomaly, respectively. Based on an anomalous AGCM, the ideal numerical experiments are also performed to illustrate the role of ISM in the east–west shift of the SAH. By considering the similar condensation heating anomalies over the ISM region to observations, we demonstrate that the model can well reproduce the observed circulation anomalies associated with the east–west shift of SAH at 200 hPa, indicating the important effect of the ISM on the zonal shift of the SAH.

Because the rainfall anomalies over China associated with the zonal shift of the SAH are mainly determined by the vertical motions, the Omega Equation at 500 hPa is diagnosed to investigate the formation mechanisms of the vertical motions. The results reveal that over North China, the anomalous sinking motion is mainly caused by both the advection of anomalous relative vorticity by the westerly basic winds and the cold advection by the anomalous northerly winds over eastern China. Over the YHR, the anomalous ascending motion is owing to the advections of the basic relative vorticity and the vorticity of the earth by

the anomalous northerly winds. The South China is covered by the WPSH, which is favorable for the descending motion over South China. Consequently, the tripole pattern of rainfall anomalies occurs with positive rainfall anomaly over the YHR and negative anomalies over North China and South China.

In our present study we propose a possible physical process through which the ISM affects the summer rainfall over China via the SAH. However, as a most pronounced signal in the interannual climate variations, the El Niño/Southern Oscillation (ENSO) can influence both the Indian and East Asian summer rainfall, leading to an apparent correlation of summer rainfall variations in the two monsoon regions (Zhang 1999; Zhang et al. 1999; Hu et al. 2005). Hu et al. (2005) separated the ISM into the ENSO-related and ENSO-unrelated parts to investigate the ENSO's role in connecting the summer rainfall over South Asia and East Asia. The ENSO-unrelated circulation anomaly (Fig. 4c in Hu et al. 2005) is similar to the circulation anomaly induced by the SAH zonal variation as shown in Fig. 5a. In addition, we calculated the correlation coefficient between the SAHI and the ENSO index defined by the sea surface temperature anomalies averaged over the NINO3.4 region (5°N–5°S, 170°–120°W). The correlation coefficient is 0.269, which is not statistically significant. Therefore, besides the influence of ENSO on both the Indian and East Asian summer rainfall, we reveal that the SAH possibly plays an important role in the effect of ISM on the East Asian summer monsoon.

Acknowledgments The authors would like to thank the anonymous reviewers for their constructive comments. This study was jointly supported by the National Natural Science Foundation of China under Grant 41221064, the International S&T Cooperation Project of the Ministry of Science and Technology of China under Grant 2009DFA21430, and the Basic Scientific Research and Operation Foundation of the CAMS under Grant 2013Z004.

References

Chen GY, Liao QS (1990) Relationship between the location features of 100 hPa South Asia High and mid-summer rainfall in China. Plateau Meteorol 9:432–438 (in Chinese)

Dai XG, Chou JF, Wu GX (2002) The teleconnection relationship between Indian monsoon and East Asian summer circulation. Acta Meterol Sin 60:544–552 (in Chinese)

Ding Q, Wang B (2005) Circumglobal teleconnection in the Northern Hemisphere summer. J Clim 18:3483–3505

Guo QY (1992) Teleconnection between the floods/droughts in North China and Indian summer monsoon rainfall. Acta Geogr Sin 47:394–402 (in Chinese)

Hu Z–Z, Wu R, Kinter LJ, Yang S (2005) Connection of summer rainfall variations in South and East Asia: role of El Niño–Southern Oscillation. Int J Climatol 25:1279–1289

Huang RH (1985) The influence of the heat source anomaly over Tibetan Plateau on the northern hemispheric circulation anomalies. Acta Meteorol Sin 43:208–219 (in Chinese)

Huang Y, Qian YF (2003) Relationship between South Asian High and summer rainfall in North China. Plateau Meteorol 22: 602–607 (in Chinese)

Jiang XA, Li T (2005) Reinitiation of the boreal summer intraseasonal oscillation in the tropical Indian Ocean. J Clim 18:3777–3795

Kripalani RH, Kulkarni A (2001) Monsoon rainfall variations and teleconnections over South and East Asia. Int J Climatol 21:603–616

Krishnamurti TN, Bhalme H (1976) Oscillations of a monsoon system. Part I. Observational aspects. J Atmos Sci 33:1937–1954

Krishnamurti TN, Daggupaty SM, Fein J, Kanamitsu M, Lee JD (1973) Tibetan high and upper tropospheric tropical circulation during northern summer. Bull Am Meteor Soc 54:1234–1249

Li T (2006) Origin of the summertime synoptic-scale wave train in the western North Pacific. J Atmos Sci 63:1093–1102

Liebmann B, Smith CA (1996) Description of a complete (interpolated) outgoing longwave radiation dataset. Bull Amer Meteor Soc 77:1275–1277

Liu YY, Ding YH (2008) Analysis and numerical simulation of the teleconnection between Indian summer monsoon and precipitation in North China. Acta Meteorol Sin 66:789–799 (in Chinese)

Liu YM, Wu GX, Liu H, Liu P (1999) The effect of spatially nonuniform heating on the formation and variation of subtropical high part III: condensation heating and South Asia high and western Pacific subtropical high. Acta Meteorol Sin 57:525–538 (in Chinese)

Liu YM, Wu GX, Liu H, Liu P (2001) Condensation heating of the Asian summer monsoon and the subtropical anticyclone in Eastern Hemisphere. Clim Dyn 17:327–338

Luo H, Yanai M (1984) The large-scale circulation and heat sources over the Tibetan Plateau and surrounding areas during the early summer of 1979. Part II: heat and moisture budgets. Mon Weather Rev 112:966–989

Luo SW, Qian ZA, Wang QQ (1982) The climatic and synoptical study about the relationship between the Qinghai-Xizang High Pressure on the 100 mb surface and the flood and drought in East China in summer. Plateau Meteorol 1:1–10 (in Chinese)

Luo Y, Zhang R, Qian W, Luo Z, Hu X (2011) Intercomparison of deep convection over the Tibetan Plateau–Asian monsoon region and subtropical North America in boreal summer using CloudSat/CALIPSO data. J Clim 24:2164–2177

Mason RB, Anderson CE (1963) The development and decay of the 100 mb summertime anticyclone over southern Asia. Mon Weather Rev 91:3–12

Peixóto JP, Oort AH (1984) Physics of climate. Rev Mod Phys 56:365–429

Sontakke N, Pant G, Singh N (1993) Construction of all-India summer monsoon rainfall series for the period 1844–1991. J Clim 6:1807–1811

Tao SY, Chen LX (1987) A review of recent research on the East Asian summer monsoon in China. In: Chang CP, Krishnamurti TN (eds) Monsoon meteorology. Oxford University Press, Oxford, pp 60–92

Tao SY, Zhu FK (1964) The 100-mb flow patterns in southern Asia in summer and its relation to the advance and retreat of the West-Pacific subtropical anticyclone over the Far East. Acta Meteorol Sin 34:385–396 (in Chinese)

Uppala SM, KÅllberg PW, Simmons AJ, Andrae U, Bechtold VDC, Fiorino M, Gibson JK, Haseler J, Hernandez A, Kelly GA, Li X, Onogi K, Saarinen S, Sokka N, Allan RP, Andersson E, Arpe K, Balmaseda MA, Beljaars ACM, Berg LVD, Bidlot J, Bormann N, Caires S, Chevallier F, Dethof A, Dragosavac M, Fisher M, Fuentes M, Hagemann S, Hólm E, Hoskins BJ, Isaksen L, Janssen PAEM, Jenne R, McNally AP, Mahfouf JF, Morcrette JJ, Rayner NA, Saunders RW, Simon P, Sterl A, Trenberth KE, Untch A, Vasiljevic D, Viterbo P, Woollen J (2005) The ERA-40 re-analysis. Quart J R Meteor Soc 131:2961–3012

Wei W, Zhang R, Wen M (2012) Meridional variation of South Asian High and its relationship with the summer precipitation over China. J Appl Meteorol Sci 23:650–659 (in Chinese)

Wu R (2002) A mid-latitude Asian circulation anomaly pattern in boreal summer and its connection with the Indian and East Asian summer monsoon. Int J Climatol 22:1879–1895

Wu R, Hu Z–Z, Kirtman PB (2003) Evolution of ENSO-related rainfall anomalies in East Asia. J Clim 16:3742–3758

Wu G, Ren S, Xu J, Wang D, Bao Q, Liu B, Liu Y (2013) Impact of tropical cyclone development on the instability of South Asian High and the summer monsoon onset over Bay of Bengal. Clim Dyn. doi:10.1007/s00382-013-1766-0

Yanai M, Esbensen S, Chu J-H (1973) Determination of bulk properties of tropical cloud clusters from large-scale heat and moisture budgets. J Atmos Sci 30:611–627

Zhang R (1999) The role of Indian summer monsoon water vapor transportation on the summer rainfall anomalies in the northern part of China during the El Niño mature phase. Plateau Meteorol 18:567–574 (in Chinese)

Zhang R (2001) Relations of water vapor transport from Indian monsoon with that over East Asia and the summer rainfall in China. Adv Atmos Sci 18:1005–1017

Zhang Q, Wu GX (2001) The large area flood and drought over Yangtze River Valley and its relation to the South Asia High. Acta Meteorol Sin 59:569–577 (in Chinese)

Zhang R, Sumi A, Kimoto M (1999) A diagnostic study of the impact of El Niño on the precipitation in China. Adv Atmos Sci 16:229–241

Zhang Q, Wu GX, Qian YF (2002) The bimodality of the 100 hPa South Asia High and its relationship to the climate anomaly over East Asia in summer. J Meteorol Soc Jpn 80:733–744

Zuo Z, Zhang R, Zhao P (2011) The relation of vegetation over the Tibetan Plateau to rainfall in China during the boreal summer. Clim Dyn 36:1207–1219